Accurate *ab initio* potential energy curve of F_2. II. Core-valence correlations, relativistic contributions, and long-range interactions

L. Bytautas
Department of Chemistry and Ames Laboratory USDOE, Iowa State University, Ames, Iowa 50011, USA

N. Matsunaga
Department of Chemistry and Biochemistry, Long Island University, Brooklyn, New York 11201, USA

T. Nagata, M. S. Gordon, and K. Ruedenberg[a)]
Department of Chemistry and Ames Laboratory USDOE, Iowa State University, Ames, Iowa 50011, USA

(Received 10 July 2007; accepted 2 October 2007; published online 26 November 2007)

The nonrelativistic, valence-shell-only-correlated *ab initio* potential energy curve of the F_2 molecule, which was reported in the preceding paper, is complemented by determining the energy contributions that arise from the electron correlations that involve the core electrons as well as the contributions that are due to spin-orbit coupling and scalar relativistic effects. The dissociation curve rises rather steeply toward the energy of the dissociated atoms because, at larger distances, the atomic quadrupole-quadrupole repulsion and spin-orbit coupling counteract the attractive contributions from incipient covalent binding and correlation forces including dispersion. © *2007 American Institute of Physics*. [DOI: 10.1063/1.2801989]

I. INTRODUCTION

The basic aim of the present series of investigations is the *ab initio* determination of molecular energies along reaction paths. Experimental information regarding energies along entire reaction paths is most complete in the case of diatomic molecules because, for many of them, full vibrational spectra have been measured with an error of less than a cm^{-1}. It has proven difficult to obtain corresponding potential energy curves accurately and fully by *ab initio* quantum mechanics. No such curve has as yet been reported for any 18-electron system such as the fluorine molecule, which is the object of the present study.

In the preceding paper,[1] we have established the nonrelativistic potential energy curve taking into account electron correlations only in the valence shell. In order to be able to make contact with physical reality at the level of accuracy of that calculation, i.e., a few tenths of a millihartree, one must also include electron correlations involving core electrons and the effects of relativity (see, e.g. Ref. 2). The latter can be obtained as the sum of the spin-orbit coupling energies[3–6] and the scalar mass-velocity-plus-Darwin (MVD) energies.[7–12] Since all of these contributions represent small correction terms, they can be calculated with less complicated wavefunctions. They are determined and added in the present paper. The dependence of the resulting full potential energies on the internuclear distance is analyzed and interpreted. The resulting energies will be used in the subsequent paper to determine the rotation vibration spectrum.

[a)]Electronic mail: ruedenberg@iastate.edu

II. *AB INITIO* ENERGIES ALONG THE DISSOCIATION CURVE

A. Correlation energy contributions involving core orbitals

The electron correlations involving core orbitals lower the total energy by about 120 mhartree, which is about 20% of the valence correlation energy at the equilibrium geometry. However, this core contribution changes only by fractions of a millihartree along the dissociation path, whereas the valence correlation energy [relative to the self-consistent-field (SCF) energy] changes by about 200 mhartree. For this reason, the energy *changes* along the reaction paths that are contributed by correlations involving the core can be calculated by simpler formalisms than those used for the correlations in the valence space in the preceding paper.[1] The method must, however, be based on a multiconfigurational reference function capable of properly representing the dissociation without a deterioration of the performance at stretched geometries. We have chosen the second-order multireference configuration interaction singles and doubles (MRCISD) approach, also called second-order CI, whose suitability for this purpose has been established by a thorough investigation of Peterson *et al.*[13] We have included the multireference analog of the Davidson correction (MRCISD+Q method), whose usefulness is well established.[14]

On the other hand, more extensive orbital basis sets are required when core as well as valence correlation energies are to be recovered reliably, as was also documented by Peterson *et al.*[13] To this end, Dunning and co-worker developed the cc-pCVXZ basis sets, systematic correlation-consistent basis sets for the simultaneous description of all

correlations, valence, and core.[15,16] We have chosen the quadruple-zeta cc-pCVQZ basis set for all calculations described in this section.

Using this approach, we have calculated the energies along the dissociation path when *all* electrons are correlated as well as the energies when only the valence electrons are correlated. The differences between these two energies yield the correlation contributions that are generated by the core electrons. All calculations were performed with the GAMESS suite of quantum chemical[17] programs.

The first step in the application of the MRCI method was the determination of the full optimized reaction space[18] (FORS) molecular orbitals

$$1\sigma_g 1\sigma_u 2\sigma_g 2\sigma_u 3\sigma_g 3\sigma_u 1\pi x_u 1\pi y_u 1\pi x_g 1\pi y_g \quad (1)$$

for the construction of the reference functions along the dissociation path. Here and in the following, we use the nomenclature of Ref. 18: complete active space SCF (CASSCF) as a generic term; FORS=CASSCF generated by a full space of valence orbitals.

When the FORS[14/8] function was MCSCF optimized to this end, the $2\sigma_g$, $2\sigma_u$ orbitals turned out to be doubly occupied for large R and, as a result, mixed with the $1\sigma_g$, $1\sigma_u$ orbitals. Such mixing interferes with the correct subsequent construction of excited configurations for the *valence-only* MRCI calculations and leads to spurious correlation energy fluctuations, as has also been observed by others.[19,20] The problem was solved by optimizing all orbitals using a reduced FORS[10/6] wavefunction involving the six active orbitals, $3\sigma_g$, $3\sigma_u$, $1\pi x_u$, $1\pi y_u$, $1\pi x_g$, and $1\pi y_g$, and the four inactive orbitals, $1\sigma_g$, $1\sigma_u$, $2\sigma_g$, and $2\sigma_u$, followed by a final Fock-matrix diagonalization among the inactive orbitals. The resulting molecular orbitals (MOs) of the list (1), expressed in terms of the cc-pCVQZ basis set, were then used for both the valence-only and the all-electron MRCI calculations.

In order to be consistent with the calculations in the preceding paper,[1] the reference functions for the valence-only MRCISD calculations were the CI wavefunctions in the full FORS[14/8] configuration space generated by the 14 valence electrons using the 8 valence orbitals, $2\sigma_g$, $2\sigma_u$, $3\sigma_g$, $3\sigma_u$, $1\pi x_u$, $1\pi y_u$, $1\pi x_g$, and $1\pi y_g$, as active orbitals, while keeping both 1σ orbitals doubly occupied. Single and double excitations were then generated by moving electrons from the eight valence orbitals into virtual orbitals.

Analogously, the reference functions for the all-electron MRCISD calculations were the CI wavefunctions in the full configuration space generated by all 18 electrons using all 10 MOs of the list (1) as active orbitals. Single and double excitations were then generated by moving electrons from all ten reference orbitals into virtual orbitals.

The results of the MRCISD and the MRCISD+Q calculations are listed in Table I for 18 points along the dissociation paths including the 13 points, at which the accurate valence correlation energies were calculated in the preceding paper.[1] As mentioned above, the core-generated correlation contributions are about 120 mhartree, but change by less than 1 mhartree. The probable superiority of the MRCISD+Q over the MRCISD approach is confirmed by the observation that the energy difference between $R=8$ Å and $R=1.411\,93$ Å (the equilibrium distance) for the MRCISD+Q calculations involving valence electron correlations (third column) is 61.43 mhartree, which is much closer to the nonrelativistic valence-correlated value of 62.56 mhartree derived from experiment (see Sec. VII B of Ref. 1 and Refs. 21 and 22) than the corresponding difference of 56.57 mhartree for the MRCISD calculations. This was already noted by Peterson *et al.*[13] One also notes that the core-correlation contribution to the binding energy (fourth column) resulting from the MRCISD+Q calculation (0.31 mhartree) is closer to the value of 0.16 mhartree reported by Peterson *et al.*[13] and by Boese *et al.*[23] than the contribution resulting from the MRCISD calculation (0.67 mhartree).

TABLE I. Determination of core-generated correlation energy contributions by means of MRCISD and MRCISD+Q calculations using cc-pCVQZ basis sets (energies in millihatrees).

R (Å)	Total energies: All electrons correlated	Total energies: Valence el's only correlated	Correlations generated by core el's
	MRCI-SD		
1.140 00	−199 364.416	−199 247.954	−116.462
1.200 00	−199 402.281	−199 286.217	−116.063
1.300 00	−199 434.216	−199 318.631	−115.585
1.360 00	−199 441.409	−199 326.011	−115.398
1.411 93	−199 443.097	−199 327.808	−115.288
1.500 00	−199 439.966	−199 324.770	−115.196
1.600 00	−199 431.755	−199 316.553	−115.201
1.700 00	−199 422.173	−199 306.891	−115.281
1.800 00	−199 413.236	−199 297.839	−115.397
2.000 00	−199 400.103	−199 284.475	−115.629
2.200 00	−199 392.979	−199 277.194	−115.785
2.400 00	−199 389.607	−199 273.738	−115.869
2.600 00	−199 388.121	−199 272.210	−115.911
2.800 00	−199 387.488	−199 271.555	−115.933
3.000 00	−199 387.230	−199 271.285	−115.945
3.200 00	−199 387.136	−199 271.184	−115.952
3.400 00	−199 387.110	−199 271.154	−115.956
8.000 00	−199 387.194	−199 271.233	−115.961
	MRCI-SD+Q		
1.140 00	−199 404.846	−199 281.555	−123.291
1.200 00	−199 443.402	−199 320.463	−122.938
1.300 00	−199 476.143	−199 353.636	−122.506
1.360 00	−199 483.581	−199 361.252	−122.329
1.411 93	−199 485.336	−199 363.119	−122.217
1.500 00	−199 482.043	−199 359.939	−122.104
1.600 00	−199 473.316	−199 351.249	−122.067
1.700 00	−199 463.016	−199 340.920	−122.096
1.800 00	−199 453.306	−199 331.146	−122.160
2.000 00	−199 438.851	−199 316.545	−122.305
2.200 00	−199 430.906	−199 308.497	−122.409
2.400 00	−199 427.106	−199 304.642	−122.464
2.600 00	−199 425.407	−199 302.918	−122.489
2.800 00	−199 424.662	−199 302.160	−122.502
3.000 00	−199 424.339	−199 301.828	−122.511
3.200 00	−199 424.207	−199 301.689	−122.519
3.400 00	−199 424.161	−199 301.637	−122.524
8.000 00	−199 424.214	−199 301.683	−122.531

TABLE II. Corrections to the nonrelativistic valence-only-correlated potential energies of F_2. For core correlations, cc-pCVQZ bases are used; for relativistic corrections, cc-pVQZ bases are used. Energies in millihartrees.

R (Å)	Core correlation	Scalar relativistic	Spin orbit	Total correlation
1.140 00	−123.291	−171.747	−0.002	−295.040
1.200 00	−122.938	−171.803	−0.003	−294.744
1.300 00	−122.506	−171.894	−0.004	−294.405
1.360 00	−122.329	−171.939	−0.005	−294.273
1.411 93	−122.217	−171.969	−0.006	−294.192
1.500 00	−122.104	−172.005	−0.009	−294.118
1.600 00	−122.067	−172.027	−0.013	−294.107
1.800 00	−122.160	−172.039	−0.028	−294.227
2.000 00	−122.305	−172.033	−0.063	−294.401
2.200 00	−122.409	−172.027	−0.145	−294.581
2.400 00	−122.464	−172.023	−0.330	−294.817
2.600 00	−122.489	−172.021	−0.652	−295.162
2.800 00	−122.502	−172.019	−0.969	−295.490
3.000 00	−122.511	−172.019	−1.139	−295.669
3.200 00	−122.519	−172.019	−1.194	−295.731
3.400 00	−122.524	−172.019	−1.204	−295.747
8.000 00	−122.531	−172.020	−1.206	−295.757
10.000 00	−122.531	−172.020	−1.206	−295.757

The MRCISD+Q values for the core-correlation contributions are also entered in the second column of Table II.

B. Scalar relativistic energy contributions

For the calculations of the relativistic scalar MVD energy corrections,[6–11] we chose the one-electron Douglas-Kroll (DK) approach[6,7] including the transformation to third order (DK3). The code in GAMESS,[17] which we have used, goes back to Nakajima and Hirao[24] and Nakajima *et al.*[25] and was further modified by Fedorov *et al.*[26]

Earlier studies[21] of diatomic binding energies had indicated that CASSCF calculations using cc-pVQZ bases yield satisfactory scalar relativistic contributions. To assess the reliability of this choice, we made DK3 calculations with a number of wavefunctions at selected points along the dissociation curve. We considered RHF-SCF, FORS[10/6], MRCISD, and MRCISD+Q wavefunctions, the latter with a FORS[14/8] as well as a FORS[18/10] reference function. The FORS orbitals determined in the previous section were used in all of these calculations, except for the RHF-SCF case. The results are given in Table III, where the various rows contain the results for various wavefunctions. The *contributions* to the potential energy curve, i.e., the values $[E(R)-E(2F)]$, are listed in columns 3–7 for five distances. The last column lists the *total* scalar relativistic contribution to the separated atoms. It is apparent that all correlated wavefunctions, including the coupled cluster result from the literature,[12] yield very similar results for the *differences* from the separated atoms, even though the total values for the latter differ by millihartrees. By contrast, the SCF/RHF values for the differences deviate markedly from the correlated values. This observation agrees with other studies[27] on similar systems.

We therefore chose FORS[10/6] wavefunctions based on the FORS orbitals of the preceding section in terms of cc-pVQZ basis sets to calculate the scalar relativistic corrections at the 18 points that we had considered along the dissociation curve in the preceding subsection. They are listed in the third column of Table II.

As was the case for the core-generated correlations, the scalar relativistic corrections have magnitudes of a few hundreds of millihartrees, but change by less than a millihartree along the dissociation path. The changes are, however, nonnegligible in the present context. These results are again consistent with previous observations.[21,22]

C. Spin-orbit coupling contributions

Ab initio methodologies for calculating the spin-orbit (SO) coupling contributions to molecular energies have been described in a number of reviews.[4–6] Most rigorous are four-component methods based on the Dirac equation. The challenges of this approach are avoided by two-component meth-

TABLE III. Scalar relativistic energy (mass-velocity-Darwin) contributions calculated with various wavefunctions. Energies in millihartrees.

Method	Basis set	$E_{MVD}(R)-E_{MVD}(\infty)$[a]					E_{MVD}
	R(Å)→	1.14	1.3	1.41193	1.6	1.8	∞[a]
				No electrons correlated			
SCF	cc-pVQZ	0.332	0.221	0.157	0.085	0.036	−173.787
				Valence electrons correlated			
MRCI[b]	cc-pCVTZ			0.058			−171.708
MRCI[b]	cc-pVQZ	0.243	0.114	0.052	0.004	−0.010	−172.584
FORS[10/6]	cc-pVQZ	0.273	0.125	0.051	−0.007	−0.019	−172.020
				All electrons correlated			
MRCI[c]	cc-pCVTZ			0.052			−174.301
CCSD(T)[d]	cc-pCVQZ			0.05			−175.00

[a]The symbol ∞ means 20 Å in all rows except the last one, where it implies twice the single atom value.
[b]Based on the FORS[14/8] reference function.
[c]Based on the FORS[18/10] reference function.
[d]Obtained as the sum of the separately calculated mass-velocity correction and Darwin correction by Helgaker, *et al.* in Ref. 12, page 852.

ods that are derived by separating the large from the small components. The most common approach[3,4,28] uses the Breit-Pauli spin-orbit operator which results from the Foldy-Wouthuysen transformation[29] of the Dirac-Breit equation truncated to second order in the fine-structure constant. The program in GAMESS (Ref. 17) uses the full one- and two-electron Breit-Pauli operators. It has been developed by Fedorov and Gordon[4] and Fedorov *et al.*[6]

Fluorine being a light atom, spin-orbit coupling essentially mixes the components of the states resulting from the Russell-Saunders coupling. Thus, its $(1s^2 2s^2 2p^5 - {}^2P)$ ground state splits into the $^2P_{1/2}$ level and the $^2P_{3/2}$ level with the energy values

$$E(^2P_{3/2}) = E(^2P) - \tfrac{1}{3}E_{\mathrm{SOS}}, \quad E(^2P_{1/2}) = E(^2P) + \tfrac{2}{3}E_{\mathrm{SOS}}, \tag{2a}$$

where

$$E_{\mathrm{SOS}} = [E(^2P_{3/2}) - E(^2P_{1/2})] = 404\ \mathrm{cm}^{-1} \tag{2b}$$

is the observed SO splitting.[28,30] At large interatomic distances, the F_2 energies will therefore converge toward three limiting values, which are evenly spaced by 404 cm^{-1}, viz.,

$$E(3/2,3/2) = E(^2P_{3/2}) + E(^2P_{3/2}) = 2E(^2P) - \tfrac{2}{3}E_{\mathrm{SOS}} = E_1, \tag{3a}$$

$$E(3/2,1/2) = E(^2P_{3/2}) + E(^2P_{1/2}) = 2E(^2P) + \tfrac{1}{3}E_{\mathrm{SOS}} = E_2, \tag{3b}$$

$$E(1/2,1/2) = E(^2P_{1/2}) + E(^2P_{1/2}) = 2E(^2P) + \tfrac{4}{3}E_{\mathrm{SOS}} = E_3. \tag{3c}$$

The corresponding molecular states are characterized as products of the atomic states, but only $M_J = M_L + M_S$ remains a good quantum number (the z axis being the internuclear axis). It can manifestly vary from −3 to 3. The numbers of configuration state functions (CSFs) with the various M_J values for the three asymptotic limits are readily deduced to be

$M_J \rightarrow$	−3	−2	−1	0	1	2	3	Total
(3/2,3/2)	1	2	3	4	3	2	1	16
(3/2,1/2)	–	2	4	4	4	2	–	16
(1/2,1/2)	–	–	1	2	1	–	–	4
Total	1	4	8	10	8	4	1	36

(4)

The zeroth-order wavefunctions of the *atomic* ^2P states are superpositions of six determinants that differ only in the occupations of the p orbitals. If we keep the $1s$ and $2s$ orbitals on both atoms also doubly occupied in the F_2 molecule, and generate the full FORS[10/6] configuration space by placing the ten remaining electrons in the six p orbitals of the two atoms F_a, F_b, then we obtain 66 determinants. This FORS can be spanned by 30 *ionic* CSFs and 36 *covalent* CSFs. The ionic configurations can be characterized as originating from the six atomic state products

$$^1S(F_a^-) \times {}^1S(F_b^+) \pm {}^1S(F_a^+) \times {}^1S(F_b^-) \rightarrow {}^1\Sigma_g^+, {}^1\Sigma_u^-, \tag{5a}$$

$$^1S(F_a^-) \times {}^1D(F_b^+) \pm {}^1D(F_a^+) \times {}^1S(F_b^-) \rightarrow {}^1\Sigma_g^+, {}^1\Sigma_u^-, {}^1\Pi_g, {}^1\Pi_u, {}^1\Delta_g, {}^1\Delta_u, \tag{5b}$$

$$^1S(F_a^-) \times {}^3P(F_b^+) \pm {}^3P(F_b^+) \times {}^1S(F_a^-) \rightarrow {}^3\Sigma_g^+, {}^3\Sigma_u^-, {}^3\Pi_g, {}^3\Pi_u. \tag{5c}$$

Thus, the ionic subspace contains 8 singlet states with a total of 12 CSFs and 4 triplet states with a total of 18 CSFs. The covalent configurations, on the other hand, can be characterized as originating from the products of the orbital holes $2p\sigma$, $2p\pi_x$, $2p\pi_y$ on the two F atoms as follows:

$$\sigma(F_a) \times \sigma(F_b) \pm \sigma(F_b) \times \sigma(F_a) \rightarrow {}^1\Sigma_g^+, {}^3\Sigma_u^+, \tag{6a}$$

$$\sigma(F_a) \times \pi(F_b) \pm \sigma(F_b) \times \pi(F_a) \rightarrow {}^1\Pi_g, {}^3\Pi_g, {}^1\Pi_u, {}^3\Pi_u, \tag{6b}$$

$$\pi(F_a) \times \pi(F_b) \pm \pi(F_b) \times \pi(F_a) \rightarrow {}^1\Sigma_g^+, {}^3\Sigma_u^+, {}^1\Sigma_u^-, {}^3\Sigma_g^-, {}^1\Delta_g, {}^3\Delta_u. \tag{6c}$$

Thus, the covalent subspace contains 6 singlet states with a total of 9 CSFs and 6 triplet states with a total of 27 CSFs.[31–33]

At the separate-atom limit, the ionic states converge to an energy that is 515 mhartree higher than that of the covalent limit, since the ionization potential and the electron affinity of F are 640 and 125 mhartree, respectively.[34]

No spin-orbit coupling exists in the molecular $^1\Sigma_g^+$ ground state at the equilibrium distance; the spin-orbit interactions set in only at large internuclear distances and they are expected to occur predominantly in the nearly separated atoms. Hence, the spin-orbit interaction matrix between all 12 covalent states listed in Eqs. (6a)–(6c) should be taken into account. However, the 12 ionic states of Eqs. (5a)–(5c), lying about half a hartree higher at the separate-atom limit, are not expected to be significantly involved in these interactions.

Quantitative calculations indeed confirm that the energy lowering of the ground state due to spin-orbit coupling obtained with all 66 FORS configurations is identical with that obtained using only the low-lying 36 configurations.

Fedorov *et al.*[6] have found that full valence space (i.e., FORS-type) wavefunctions as well as MRCISD wavefunctions gave equally good agreement with experimental values in molecules of light elements, and they infer that *dynamic* correlation has a relatively small effect on SO coupling in these systems. We confirmed their observations by performing SO coupling calculations for F_2 at selected geometries with cc-pVTZ basis sets. Use of FORS[10/6] wavefunctions and MRCISD wavefunctions yielded indeed near-identical results, the difference being, e.g., 0.01 mhartree at 2.2 Å and 0.005 mhartree at 2.6 Å as well as 3 Å. As another test, we calculated the SO coupling in F_2 at an internuclear distance of 8 Å, using the FORS[10/6] wavefunction and the quadruple-zeta cc-pVQZ bases. We obtained, in fact, the asymptotic results predicted by Eqs. (3a)–(3c) and (4): The energies of the CSFs converge to three limits, those converging to the same limit differing from each other by less than 1 cm^{-1} and the three limits differing from the pre-SO-coupling energy $2E(^2P)$ by

$$E_1 - 2E(^2P) = -\tfrac{2}{3}E'_{\mathrm{SOS}},$$

$$E_2 - 2E(^2P) = \tfrac{1}{3}E'_{\mathrm{SOS}}, \tag{7}$$

$$E_3 - 2E(^2P) = \tfrac{4}{3}E'_{\mathrm{SOS}},$$

with $E'_{\mathrm{SOS}}=396$ cm^{-1}, which deviates only by 8 cm^{-1} from the experimental value of Eq. (2b). The number of converging CSFs and their M_J values also agree with Eq. (4).

We chose the FORS[10/6] wavefunction with Dunning's cc-pVQZ basis for the calculation of the spin-orbit coupling corrections along the entire dissociation curve of F_2. Moreover, for simplicity we used only the 36-dimensional covalent subspace of the full 66-dimensional FORS[10/6] space since, as discussed above, the inclusion of ionic states has no effect on the magnitude of the spin-orbit coupling.

The first step was the determination of appropriate orbitals. They were obtained by optimizing a fully state-averaged MCSCF wavefunction involving all 18 CSFs with $M_S=0$ in the 36-dimensional covalent space of Eqs. (6a)–(6c). This state averaging yields equivalent orbitals, which are essential for obtaining good spin-orbit corrections, just as three equivalent p orbitals are required to obtain correct SO coupling corrections in the F atom.

With these orbitals, the wavefunctions of the 36 CSFs of the covalent FORS states of Eqs. (6a)–(6c) were then determined by a CI calculation and, subsequently, the Breit-Pauli spin-orbital coupling matrix among *these* 36 CSFs was diagonalized. The difference between the ground state energies with and without spin-orbit coupling furnished then the spin-orbital coupling correction to the electronic energy. The values of these energy lowerings due to SO coupling at the 18 points listed in Table II are entered in the fourth column of that table.

The fifth column of Table II gives the total energy correction, i.e., the sum of the core-generated correlations, the scalar relativistic contributions, and the spin-orbit coupling energies, which are listed in the preceding three columns.

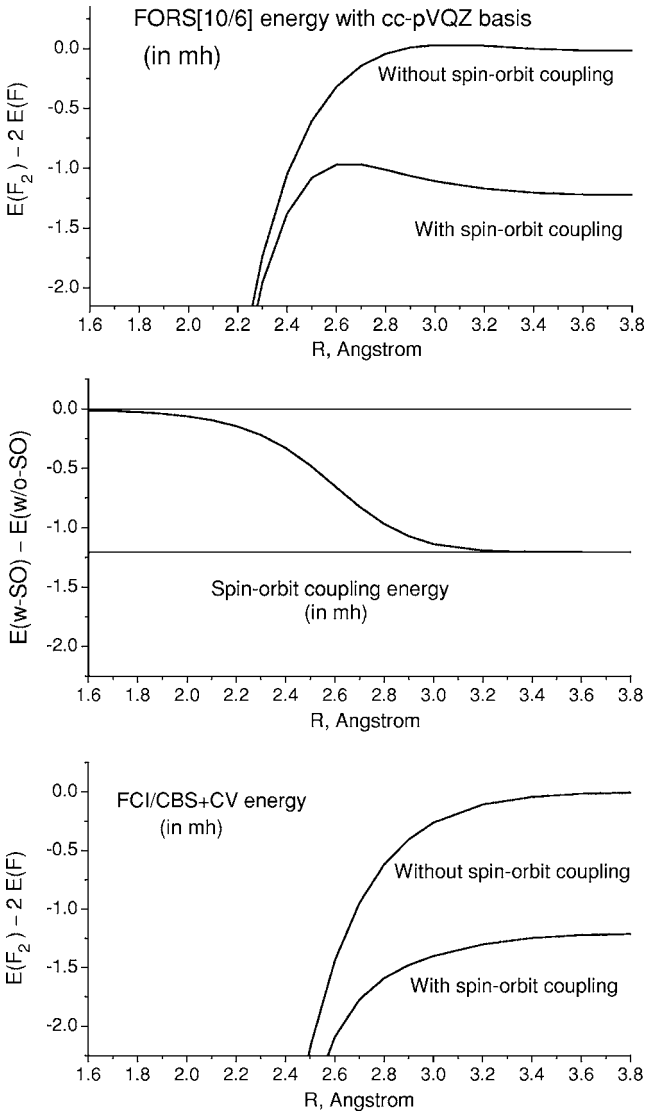

FIG. 1. Spin-orbit (SO) coupling in F_2 as function of the internuclear distance (the equilibrium distance is at 1.411 93 Å). Upper panel: FORS[10/6] calculations to determine the SO correction. Middle panel: The SO correction function=difference between the curves of the upper panel. Lower panel: Application of the SO correction of the middle panel to the fully correlated and CBS extrapolated energy curve.

The variation of the effect of spin-orbit coupling along the entire dissociation curve is illustrated in Fig. 1. The top panel displays plots of the FORS[10/6] calculations using cc-pVQZ bases with and without SO coupling. The middle panel displays a plot of the difference between the two plots of the top panel, i.e., the SO coupling correction. On the lower panel, the upper curve displays the complete basis set (CBS) limit of the full CI energy including core correlations and the lower curve represents the final result when the SO correction of the middle panel is added to the upper curve of the lower panel.

It should be noted that the gradual disappearance of the spin-orbit coupling when the two F atoms approach each other results in a *repulsive force* opposing the attractive bonding interactions between the atoms.

TABLE IV. The *ab initio* potential energy curve of F_2. Listed in all columns are the values of $[E(R)-E(8\ \text{Å})]$ [The energy at $R=8$ Å represents the (F+F) dissociation limit.] Energies are in millihartrees.

R (Å)	No Relat., no core correl.[a]	Core correlation[b]	Scalar Relativistic[b]	Spin orbit coupl.[b]	Total corrections	*Ab initio* PES curve
1.140 00	18.060	−0.760	0.273	1.204	0.717	18.777
1.200 00	−20.360	−0.408	0.217	1.203	1.012	−19.348
1.300 00	−53.230	0.024	0.125	1.202	1.352	−51.878
1.360 00	−60.620	0.202	0.081	1.201	1.484	−59.136
1.411 93	−62.350	0.314	0.051	1.200	1.564	−60.786
1.500 00	−59.270	0.427	0.015	1.198	1.639	−57.631
1.600 00	−50.710	0.463	−0.007	1.194	1.650	−49.060
1.800 00	−30.300	0.371	−0.019	1.179	1.530	−28.770
2.000 00	−15.590	0.225	−0.013	1.144	1.356	−14.234
2.200 00	−7.390	0.122	−0.007	1.061	1.176	−6.214
2.400 00	−3.530	0.066	−0.003	0.877	0.940	−2.590
2.800 00	−0.640	0.029	0.000	0.237	0.267	−0.373
8.000 00	0.000	0.000	0.000	0.000	0.000	0.000

[a]Complete basis set limit of nonrelativistic values with only valence electrons being correlated. Derived from Table X of the preceding paper (Ref. 1).
[b]Derived from Table II of the present paper.

III. *AB INITIO* POTENTIAL ENERGY SURFACE

A. *Ab initio* dissociation curve

It is seen from Table II that core correlations and scalar relativistic effects add up to corrections of about 300 mhartree, when using quadruple-zeta basis sets. Extrapolation to the full basis set limit would change these values by amounts in excess of a few millihartrees. However, the comparison with experiment to be made in the subsequent paper involves only the dissociation curve, i.e., the differences $[E(R)-E(\infty)]$. As was already noted in Secs. II A and II B, these differences change only by fractions of a millihartree along the dissociation curve, so that the complete basis set extrapolation does not have to be applied to them.

Table IV collects all our quantitative *ab initio* results that pertain to the dissociation curve $[E(R)-E(\infty \equiv 8\ \text{Å})]$. The second column lists the nonrelativistic valence-only-correlated energies that are deduced from Table X of the preceding paper[1] by the method of the correlation energy extrapolation by intrinsic scaling (CEEIS). The third, fourth, and fifth columns list the core-generated correlations, the scalar relativistic effects, and the spin-orbit coupling, respectively, which are deduced from Table II above. The sixth column lists the sum of these corrections. The final column lists the sum of the second and the sixth columns, i.e., the *ab initio* potential energy curve of the fluorine molecule.

In the preceding paper we had, however, noted that, due to small uncertainties in the CEEIS extrapolations, small variations are possible in the valence correlation energies (mostly less than 0.1 mhartree, a few between 0.1 and 0.2 mhartree), and we had considered the corresponding small variations that result in the values in the last column of Table X of the preceding paper. We therefore consider them also for the *ab initio* potential curve in the last column of the present Table IV. The pertinent deviations were listed in Table XI of the preceding paper.[1] Thus, we shall also consider the four additional potential energy curves that are obtained by applying these additive deviations to the potential energy values listed in the last column of Table IV. We shall denote the corresponding five variants of our potential energy curve as EXTR1c, EXTR2c, EXTR3c, EXTR4c, and EXTR5c, where we have taken the labels from Table XI of the preceding paper[1] and added the letter "c" to indicate the addition of the correction terms listed in the sixth column of the present Table IV.

As a first test of the quality of the *ab initio* potential energy curve given in the last column of Table IV, we compare it with the potential energy curve derived by Colbourn *et al.*[35] from the experimental spectroscopic data using the RKR procedure[36–38] (see also Refs. 39–42). In Fig. 2, the 47 values of the RKR curve[35] are shown as solid dots, while the

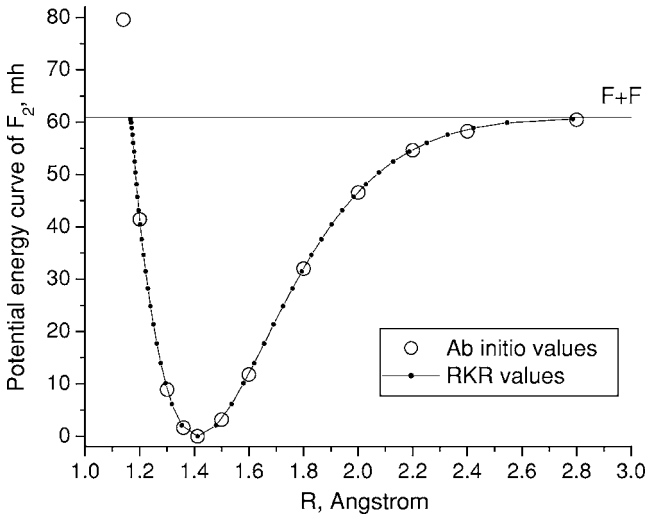

FIG. 2. Potential energy curve of F_2. Filled circles (47 values): RKR values of Ref. 35. Large open-circles (12 values): *ab initio* values of Table IV shifted up by 60.786 mhartree to be consistent with the display of RKR data in Ref. 35.

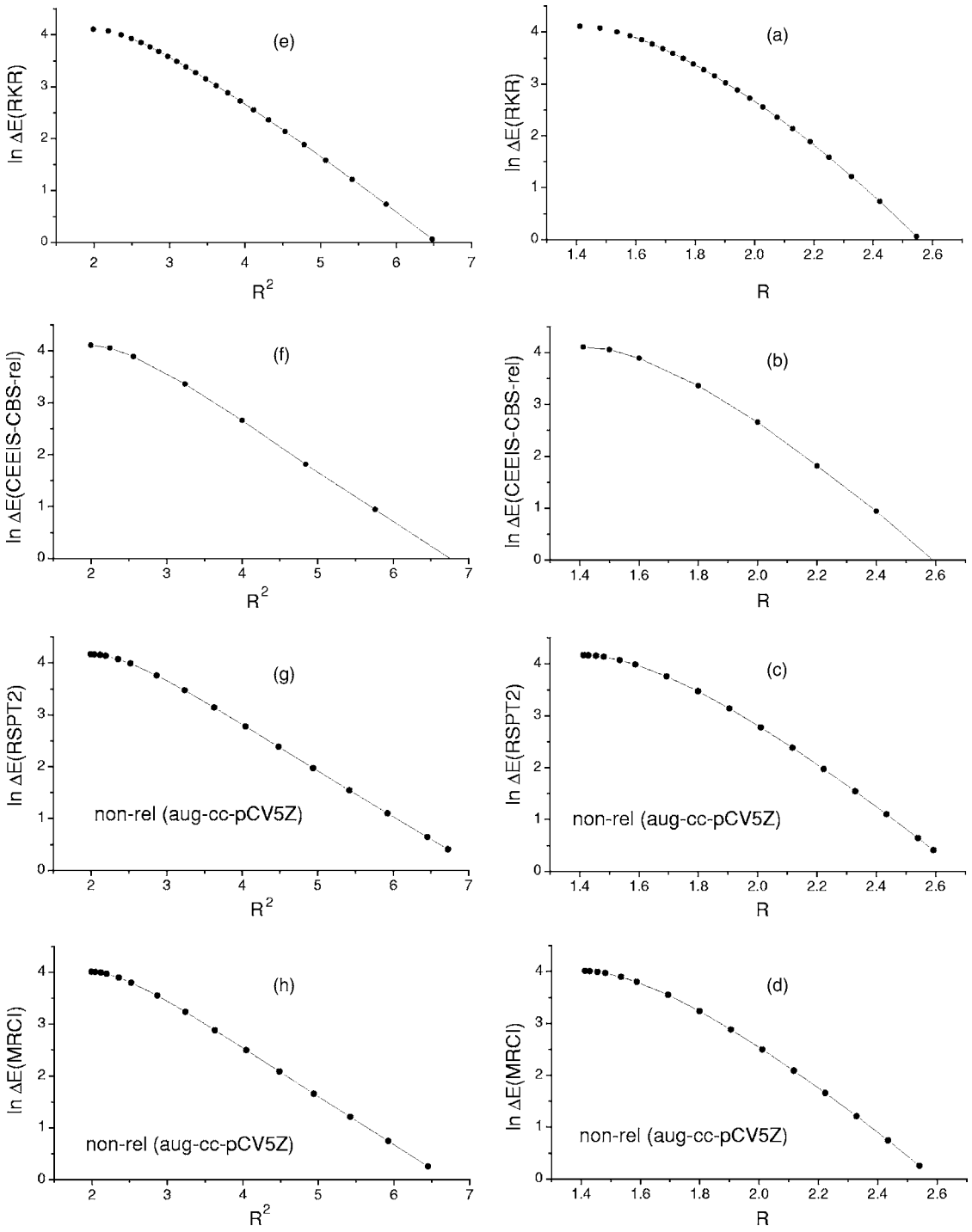

FIG. 3. The rise of the potential energy curves from the equilibrium distance (1.411 93 Å) toward the dissociation limit. Plotted is the natural logarithm of $\Delta E=[V(\infty)-V(R)]$ vs R on the right panels [(a)–(d)] and vs R^2 on the left panels [(e)–(h)]. First row [(a) and (e)]: RKR potential of Ref. 35. Second row [(b) and (f)]: the present potential (fully correlated+CBS limit+relativity). Third row [(c) and (g)]: Raleigh-Schrödinger second order perturbation theory (fully correlated, no relativity, augmented quintuple zeta basis). Fourth row [(d) and (h)]: multireference configuration interaction.

ab initio values are indicated by open circles. The agreement between the two data sets is manifestly good. The quality of the RKR curve suffers, as is well known,[39] when its value comes close to the dissociation energy at about 1.16 and 2.79 Å.

B. The dissociation curve of F_2 exhibits a Gaussian decay

Surprisingly, the dissociation curve exhibits a *Gaussian decay* as the internuclear distance increases from the equilibrium geometry of 1.411 93 to 2.8 Å. This remarkable feature is documented in Fig. 3, which displays plots of the natural logarithms of the absolute values of the energy differences $[E(R)-E(\infty)]$ of the following four dissociation curves versus R as well as R^2.

(1) Top panel: The "experimental" RKR curve of Colbourn *et al.*[35]

(2) Second panel from top: The curve given in the last column of Table IV of the present investigation.

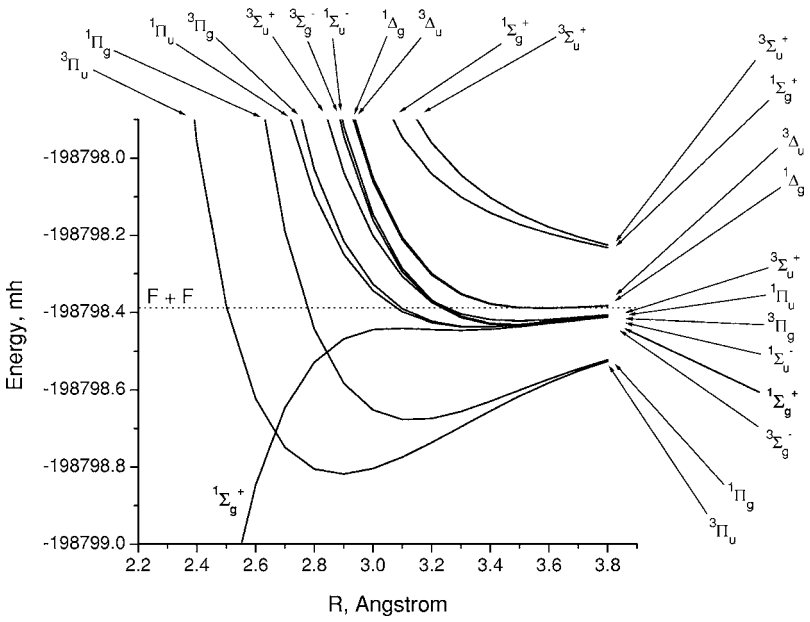

FIG. 4. The 12 covalent states (containing 36 CSFs) in the FORS[10/6] space that are included in the spin-orbit interaction coupling calculations. The energy curves are calculated at the FORS[10/6] level with a cc-pVTZ basis. (The slight dip at about 3.3 Å is due to state averaging here and is absent in Fig. 7.)

(3) Third panel from top: The curve obtained by a multireference second order Raleigh-Schrödinger perturbation theory that correlates all electrons of the FORS[14/8] reference function, using augmented quintuple-zeta (aug-cc-pCV5Z) basis sets.
(4) Bottom panel: The curve of a MRCISD calculation correlating all orbitals of the FORS[14/8] reference function using augmented quintuple-zeta (aug-cc-pCV5Z) basis sets.

The two last mentioned calculations were performed with the MOLPRO code.[43]

For each method of calculation, the left panel shows the plot versus R^2 and the right panel shows the plot versus R. It is manifest that all of these potential energy curves conform much more closely to a Gaussian than to an exponential decay up to about 3 Å. They certainly do not exhibit an inverse-power decay up to that point.

IV. LONG-RANGE DEPENDENCE ON THE INTERNUCLEAR DISTANCE

The highest experimental vibrational level of F_2 intersects the experimental dissociation curve, which Colbourn *et al.*[35] derived by the RKR method, at about 2.8 Å, i.e., twice the equilibrium distance. On the other hand, beyond this distance, the possible error in the *ab initio* calculations of the preceding paper,[1] becomes comparable to the value of the potential energy itself. Thus, neither the spectroscopic nor the theoretical information presently available allows precise conclusions regarding the potential energy surface (PES) values beyond about 3 Å.

An analysis of the long-range interactions is nonetheless relevant because it will shed light on the reasons for the steep Gaussian decay noted in the preceding section. We shall argue that, as the atoms approach each other, the descent of the potential energy curve to the minimum is at first impeded by two repulsive forces: one is due to the loss of spin-orbit coupling, the other is due to quadrupole-quadrupole interactions. The descent then occurs very rapidly as the exponentially increasing orbital overlap generates covalent attractions through electron sharing.

A. Closer examination of spin-orbit coupling

The spin-orbit coupling interactions described in Sec. II C involved the 12 covalent states enumerated in Eqs. (6a)–(6c). The long-range ($R > 2.5$ Å) variation of their energies with the internuclear distance *before* SO coupling is exhibited in Fig. 4. These plots were obtained with FORS[10/6] wavefunctions using cc-pVTZ basis sets. Very similar plots would result with the cc-pVQZ basis sets. (Note that the total range from the bottom to the top of the energy scale is only 1 mhartree). While at 3.8 Å, the 12 states still spread over an energy range of 0.3 mhartree, this range shrinks to less than 0.007 mhartree at 8 Å.

The figure exhibits several remarkable features. Upon approach from large distances, the $^1\Sigma_g^+$ state, which is the ground state at equilibrium and the real object of our interest, begins the bonding descent only at about 2.9 Å, whereas the $^1\Pi_g$ and $^3\Pi_u$ states start to descend already at distances larger than 4 Å even though they are repulsive at shorter distances. As a consequence the Π states cross the $^1\Sigma_g^+$ state between 2.6 Å and 3 Å. It is furthermore striking that, at the distance of 3.8 Å, the 12 covalent states have coalesced into four distinct limiting values. We shall see in the next section that both features are manifestations of the quadrupole-quadrupole interactions between the two F atoms at large distances.

The energy curves that result from performing the spin-orbit coupling calculations for the 12 states of Fig. 4 are shown in Fig. 5. Only the lowest five states (eight CSFs) are displayed. Each of them is identified by $\Omega = |M_J|$, which remains a good quantum number, as mentioned in Sec. II C. The symmetry distinction g versus u manifestly remains a rigorous classification as well. In the figure, each spin-orbit coupled state is moreover characterized by the states that are its main contributors.

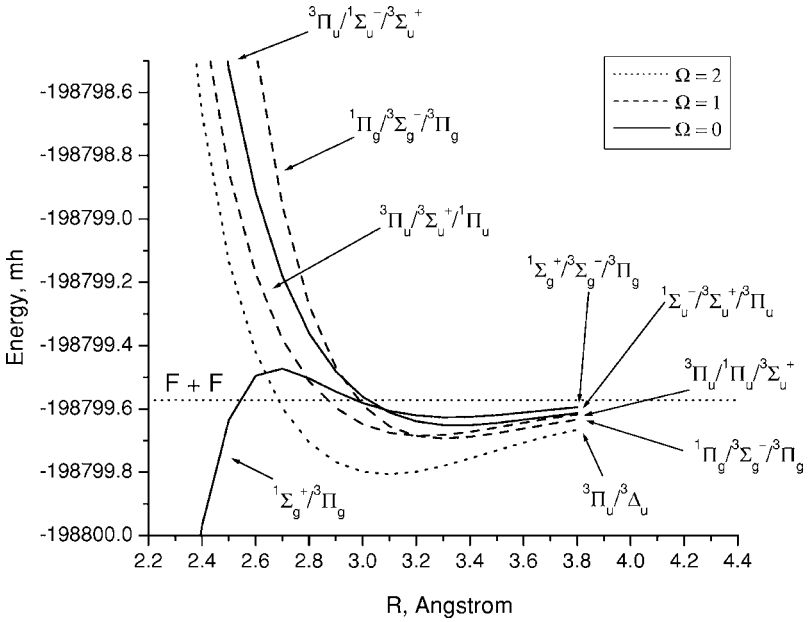

FIG. 5. Energy curves of the four lowest states (8 CSFs) that result from the spin-orbit interactions between the 12 states in the covalent FORS[10/6] space shown in Fig. 4. The states are labeled by the value of $\Omega=|M_J|=|M_L+M_S|$, by g and u, and by their main contributing states (which were displayed in Fig. 4) in order of importance. Since these contributors can change along the curve, they are shown at both ends.

The ground state at shorter distances is designated as $^1\Sigma_g^+/^3\Pi_g$, indicating that it is dominated by the $^1\Sigma_g^+$ state with a small admixture of the $^3\Pi_g$ state. At the right end, its curve is designated by the symbol $^1\Sigma_g^+/^3\Sigma_g^-/^3\Pi_g$ indicating that for larger distances (beyond 3.1 Å) a $^3\Sigma_g^-$ admixture is actually stronger than the $^3\Pi_g$ admixture. The crossing between the $^1\Sigma_g^+$ state and the lowest $^3\Pi_u$ state survives the spin-orbit interaction because of the g-u difference. The crossing between the $^1\Sigma_g^+$ state and the lowest $^1\Pi_g$ state survives the spin-orbit interaction because of the difference in M_J.

The energy *difference* between the $^1\Sigma_g^+/^3\Pi_g$ curve in Fig. 5 and the lowest $^1\Sigma_g^+$ curve in Fig. 4 is the ground state spin-orbit coupling. The upper panel in the earlier discussed Fig. 1 displays the analogous two curves obtained with the quadruple-zeta basis sets. The comparison of the corresponding curves in Figs. 4 and 5, as well as those in Fig. 1, clearly shows that spin-orbit coupling has a repulsive effect on the ground state potential energy curve.

It would seem likely that the addition of dynamic electron correlation will not change the *relative* positioning of the two lowest curves in Fig. 5, i.e., $(^1\Sigma_g^+/^3\Pi_g)$ and $(^3\Pi_u/^3\Delta_u)$. In the context of nuclear dynamics, there exists therefore the possibility of a nonadiabatic coupling between these two states in the neighborhood of their intersection. If so, such nonadiabatic interactions may influence the highest vibrational levels of the ground state.

B. Quadrupolar electrostatic interactions and dispersion forces

In its $(1s^22s^22p^5-{}^2P)$ ground state, the F atom has a quadrupolar density. As was already discussed by Knipp[44] in 1938, there exists therefore a quadrupole-quadrupole interaction $(\sim R^{-5})$ between the atoms in F_2 at large distances, in addition to the London dispersion $(\sim R^{-6})$ interaction. Neglecting terms of higher order, one would therefore expect a long-range potential of the form

$$V_{\mathrm{LR}}(R) = D - C_5/R^5 - C_6/R^6 - , \ldots , \tag{8}$$

with D being the dissociation energy.[45–47]

The interaction between the quadrupoles depends on their alignment. If they are coaxially aligned, they repel each other, since here (see, e.g., Ref. 48)

$$-C_5 = 6\Theta^2 = 6(0.731)^2 \text{ a.u.} = 133.0 \text{ mhartree Å}^5, \tag{9a}$$

where we have inserted the quadrupole moment Θ calculated for the F atom by Medved *et al.*[49] using the CASPT2 method. If, on the other hand, the quadrupole axis of one atom coincides with the internuclear axis while the quadrupole axis on the other atom is perpendicular to it, then one has an attraction,[48] viz.,

$$-C_5 = -3\Theta^2 = -3(0.731)^2 \text{ a.u.} = -66.5 \text{ mhartree Å}^5. \tag{9b}$$

Dispersion, on the other hand, is always attractive. Chu and Dalgarno[50] have obtained the dispersion coefficient C_6 for F_2 by imaginary frequency integration of the square of the atomic polarizability of the F atom, which they calculated by time-dependent density functional theory. They found[50]

$$C_6 = 9.52 \text{ a.u.} = 209.0 \text{ mhartree Å}^6. \tag{10}$$

The long-range potentials V_{LR} that result by inserting the values (9a), (9b), and (10) into Eq. (8) are plotted in Fig. 6; the upper panel corresponding to the repulsive quadrupole alignment and the lower panel corresponding to the attractive quadrupole alignment. For the coaxial alignment, the quadrupolar repulsion is seen to dominate everywhere in the range of interest. Around 3 Å, the sum of the two terms is repulsive by about 0.25 mhartree. The possible competition between quadrupolar and dispersion interactions was already considered by Chang.[45]

In the lowest $^1\Sigma_g^+$ state, the quadrupoles of the two F atoms are coaxially aligned[51–53] and hence repel each other. In the lowest two Π states, on the other hand, the quadrupole

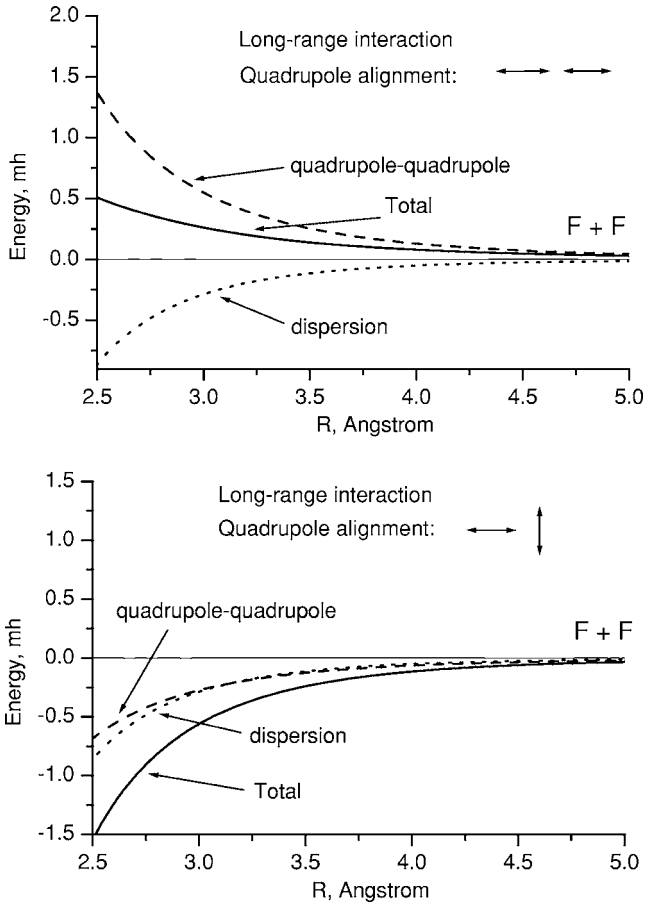

FIG. 6. Long-range quadrupole and London dispersion interactions in F_2. Upper panel: Repulsive alignment between the fluorine quadrupoles in the $^1\Sigma_g^+$ ground state. Lower panel: Attractive alignment of the fluorine quadrupoles in an excited state of Π symmetry.

axis of one atom coincides with the internuclear axis while that of the other atom is perpendicular to it so that an attraction results. This is the reason for the behavior of these states at large distances, which was discussed in the preceding section. Furthermore, Knipp[44] predicted already in 1938 that the lowest 12 covalent states in F_2 would coalesce into four energy levels in exactly the way we find at 3.8 Å, as shown in Fig. 4, and he furthermore predicted exactly the number and the symmetry characteristics of the states for each of the four groups, as they are identified in Fig. 4.

C. Resolution of the total energy of the ground state

The influence of the various contributions to the potential energy curve is exhibited in Fig. 7, where all curves are shifted to zero energy value at the separated atom limit. Within the quantum mechanical framework, the multipole interaction is expected to be embedded in the $^1\Sigma_g^+$ configuration of the FORS of Eq. (6a). The solid curve labeled FORS[14/8] represents the CBS limit of this full-valence-space energy. The *light* solid line displays the quadrupole-quadrupole repulsion from Fig. 6. It is apparent that this repulsion is reflected in the long-range repulsive character of the FORS energy. This quantitative observation, in conjunction with the theoretically predicted fusing of the 12 valence states into four groups and the crossing with the Π states

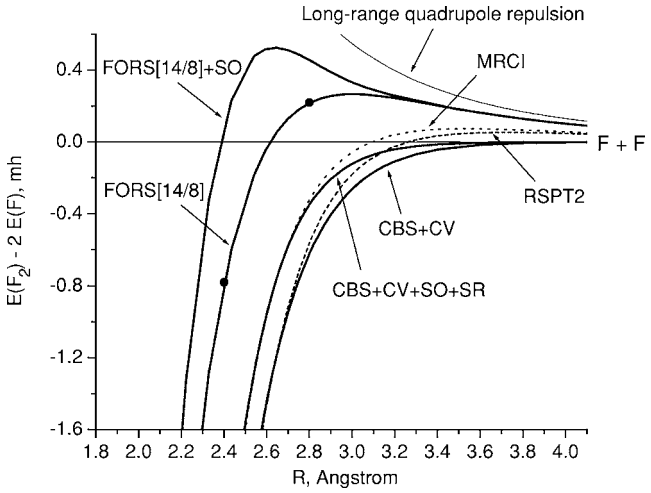

FIG. 7. Heavy solid lines: Potential energy curves embodying various contributions of the present calculations, as indicated (see text). Dashed lines: Comparison calculations using simpler dynamic correlation descriptions, as indicated (see text). Light solid line: Quadrupole-quadrupole repulsion for coaxial alignment from upper panel of Fig. 6. The curve labeled FORS[14/8] is calculated using the aug-cc-pCV5Z basis. The two heavy dots on this curve are the values of the CBS limit at 2.4 and 2.8 Å reported in Table I of preceding paper (Ref. 1). The solid curve is thus the CBS limit on the scale of the figure.

discussed in the preceding paragraph, leaves no doubt about the influence of the quadrupolar forces on the shapes of the potential energy curves at long range.

The solid line labeled {FORS[14/8]+SO} is obtained by adding the spin-orbit interaction to the FORS[14/8] limit. It shows how the SO coupling increases the repulsive character of the potential energy curve at this level of nondynamic correlation.

The solid curve labeled CBS+CV represents the nonrelativistic potential energy containing all-electron correlations but no SO coupling. It shows that the sum of all *dynamic* correlations overcomes the repulsive character found at the nondynamic correlation level. This observation is confirmed by the two dashed lines: one, labeled RSPT2, represents a multireference second-order Raleigh-Schrödinger perturbation calculation; the other, labeled MRCI, represents a MRCISD calculation. Both correlate all electrons of a FORS[14/8] reference function and use augmented quintuple-zeta (aug-cc-pCV5Z) basis sets. These two curves show that dynamic correlations almost remove the repulsive hump of the FORS[14/8] approximation, although they are not as effective as the CEEIS full CI calculations.

Finally, addition of SO coupling and the scalar relativistic contributions yields the curve labeled CBS+CV+SO+SR, which is the actual *ab initio* potential energy curve. It is apparent that the energy lowering due to the dynamic correlations eliminates the repulsive effects of quadrupole interactions as well as spin-orbit coupling. But even so, upon approach from large distances these two repulsive contributions initially counteract the attractive forces so that the descent toward the minimum is at first checked and then occurs more steeply than it would have been without this initial impediment. This makes the Gaussian-type distance dependence noted above understandable.

Even though, for $R>2.8$ Å, our dynamic correlation calculations do not yield the potential with an error <0.1 mhartree, the discussed features of Fig. 7 manifestly exhibit that there exists a competition between the quadrupole-quadrupole repulsion, the spin-orbit-coupling repulsion, and the attractions due to dynamic correlations in this long-range region. These competing influences make it difficult to predict the quantitative long-range dependence of the potential energy curve on the internuclear distance exactly at this time. In this light, it is understandable why calculations with shorter basis sets and/or simpler correlation treatments may yield a slight hump on the potential energy curve for $R>3$ Å, as is, e.g., exhibited by the MRCI curves on Fig. 7, and as was also found by Lie and Clementi[54] as well as by Li and Paldus,[55] who generated full CI energies with a double-zeta basis.

We also note that, while the total electron correlation eliminates the "precorrelation hump," the discussion in Sec. IV B showed that the r^{-6}-type dispersion forces alone are unable to overcome the quadrupole repulsions. One thus has to infer that the total correlation must embody stronger attractions than the standard dispersion terms or, alternatively, that the value of the C_6 coefficient calculated in Ref. 50 is too small. We are currently examining this question in greater detail.

V. CONCLUSIONS

In the preceding paper,[1] the nonrelativistic potential energy curve of F_2 had been determined within a few tenths of a millihartree. In the present paper, the contributions of electron correlations involving the core, of spin-orbit coupling and of scalar relativistic effects have been added in order to be able to make contact with physical reality. These contributions to the potential energy curve are found to have magnitudes of up to 1.65 mhartree. They significantly improve the overall quality of the *ab initio* potential energy curve, as has also been observed by other researchers, who emphasize the importance of these higher-order contributions.[56–60] The resulting energies agree with the experimentally deduced RKR curve within the accuracy of the present calculations. The diagonal non-Born-Oppenheimer corrections have not been considered here since several studies[58,61,62] imply that their contributions to the potential curve of F_2 are negligible. In particular, Gauss *et al.*[62] have recently demonstrated that, while the diagonal Born-Oppenheimer contribution (DBOC) to the total energy of F_2 has a value of 1174.8 cm^{-1} at the equilibrium distance, it contributes less than 1 cm^{-1} to the dissociation energy since the sum of the DBOCs for two fluorine atoms is 1175.6 cm^{-1}.

Notably, it is found that the rise of the potential energy curves from the minimum to the dissociation limit is rather steep and, in fact, exhibits a Gaussian shape between the equilibrium distance and the long-range region. This is shown to be due to the fact that, at larger distances where the overlap-dependent covalent attractions become weak, quadrupole-quadrupole repulsions as well as spin-orbit coupling repulsions counteract the dispersion attractions, dynamic electron correlations, and incipient covalent bonding. These results suggest a reexamination of the notion[35] that, in the $^1\Sigma_g$ ground states of dihalogen molecules, dispersion forces dominate the long-range potential. Also, the possibility of minute hump in the $^1\Sigma_g$ curve cannot be entirely excluded. We shall return to these questions in a subsequent study.

The aforementioned quadrupole-quadrupole interactions are also responsible for the fact that, at large distances, a $^3\Pi_u$ state lies below the nominal $^1\Sigma_g$ ground state and crosses it at about twice the equilibrium distance. A nonadiabatic coupling (in combination with spin-orbit interaction) between these two states is therefore a possibility, which may be relevant for nuclear dynamics including the highest vibrational levels.

ACKNOWLEDGMENTS

The authors thank Dr. Dmitri G. Fedorov for generously sharing his experience and knowledge regarding spin-orbit calculations. They thank Dr. Michael W. Schmidt for his lively interest, his stimulating critique, and his many valuable suggestions. They thank Professor Donald Truhlar for raising the question of quadrupole interactions and Dr. Michael Schmidt for bringing the paper by J. Knipp on this subject to the authors' attention. They furthermore thank Professor Anthony Stone, Professor Alexander Dalgarno, and Professor Robert J. Le Roy for their helpful correspondence regarding long-range forces. Instructive discussions with Professor R. Benny Gerber, Professor Ralph Jaquet, Professor Werner Kutzelnigg, and Professor Eugen Schwarz are also gratefully acknowledged. The present work was supported by the Division of Chemical Sciences, Office of Basic Energy Sciences, U.S. Department of Energy under Contract No. DE-AC02-07CH11358 with Iowa State University through the Ames Laboratory.

[1] L. Bytautas, T. Nagata, M. S. Gordon, and K. Ruedenberg, J. Chem. Phys. **127**, 164317 (2007).
[2] P. R. Taylor, *Lecture Notes in Quantum Chemistry*, edited by B. O. Roos (Springer-Verlag, Berlin, 1992), Vol. 58, p. 325.
[3] T. R. Furlani and H. F. King, J. Chem. Phys. **82**, 5577 (1985).
[4] D. G. Fedorov and M. S. Gordon, J. Chem. Phys. **112**, 5611 (2000).
[5] C. M. Marian, Rev. Comput. Chem. **17**, 99 (2001).
[6] D. G. Fedorov, S. Koseki, M. W. Schmidt, and M. S. Gordon, Int. Rev. Phys. Chem. **22**, 551 (2003).
[7] M. Douglas and N. M. Kroll, Ann. Phys. (N.Y.) **82**, 89 (1974).
[8] R. D. Cowan and D. C. Griffin, J. Opt. Soc. Am. **66**, 1010 (1976).
[9] B. A. Hess, Phys. Rev. A **33**, 3742 (1986).
[10] A. Wolf, M. Reiher, and B. A. Hess, J. Chem. Phys. **117**, 9215 (2002).
[11] T. Nakajima and K. Hirao, Monatsch. Chem. **136**, 965 (2005).
[12] T. Helgaker, P. Jørgensen, and J. Olsen, *Molecular Electronic-Structure Theory* (Wiley, Chichester, 2000).
[13] K. A. Peterson, A. K. Wilson, D. E. Woon, and T. H. Dunning, Jr., Theor. Chem. Acc. **97**, 251 (1997).
[14] S. R. Langhoff and E. R. Davidson, Int. J. Quantum Chem. **8**, 61 (1974); M. R. A. Blomberg and P. E. M. Siegbahn, J. Chem. Phys. **78**, 5682 (1983); J. Simons, J. Phys. Chem. **93**, 626 (1989).
[15] T. H. Dunning, Jr., J. Chem. Phys. **90**, 1007 (1989).
[16] D. E. Woon and T. H. Dunning, Jr., J. Chem. Phys. **103**, 4572 (1995).
[17] M. W. Schmidt, K. K. Baldridge, J. A. Boatz, S. T. Elbert, M. S. Gordon, J. H. Jensen, S. Koseki, N. Matsunaga, K. A. Nguyen, S. J. Su, T. L. Windus, M. Dupuis, and J. A. Montgomery, J. Comput. Chem. **14**, 1347 (1993); M. S. Gordon and M. W. Schmidt, in *Theory and Applications of Computational Chemistry: The First Forty Years*, edited by C. E. Dykstra, G. Frenking, K. S. Kim, and G. E. Scuseria (Elsevier, Amsterdam, 2005), p. 1167.

[18] K. Ruedenberg, M. W. Schmidt, M. M. Gilbert, and S. T. Elbert, Chem. Phys. **71**, 41 (1982).
[19] K. A. Peterson, R. A. Kendall, and T. H. Dunning, Jr., J. Chem. Phys. **99**, 9790 (1993).
[20] H.-J. Werner and P. J. Knowles, J. Chem. Phys. **94**, 1264 (1991).
[21] D. Feller and J. A. Sordo, J. Chem. Phys. **113**, 485 (2000).
[22] L. Bytautas and K. Ruedenberg, J. Chem. Phys. **122**, 154110 (2005).
[23] A. D. Boese, M. Oren, O. Atasoylu, J. M. L. Martin, M. Kállay, and J. Gauss, J. Chem. Phys. **120**, 4129 (2004).
[24] T. Nakajima and K. Hirao, Chem. Phys. Lett. **302**, 383 (1999).
[25] T. Nakajima, K. Koga, and K. Hirao, J. Chem. Phys. **112**, 10142 (2000).
[26] D. G. Fedorov, T. Nakajima, and K. Hirao, Chem. Phys. Lett. **335**, 183 (2001).
[27] C. W. Bauschlicher, Jr., J. Phys. Chem. A **104**, 2281 (2000).
[28] A. Nicklass, K. A. Peterson, A. Berning, H.-J. Werner, and P. J. Knowles, J. Chem. Phys. **112**, 5624 (2000).
[29] L. L. Foldy and S. A. Wouthuysen, Phys. Rev. **78**, 29 (1950).
[30] C. E. Moore, *Atomic Energy Levels*, Natl. Bur. Stand. Ref. Data Ser., Natl. Bur. Stand. (U.S. Ciac. No. 35) (U.S. GPO, Washington, DC, 1971).
[31] E. Wigner and E. E. Witmer, Z. Phys. **51**, 859 (1928).
[32] F. Hund, Z. Phys. **63**, 723 (1930).
[33] R. S. Mulliken, Rev. Mod. Phys. **4**, 1 (1932).
[34] See J. Emsley, *The Elements* (Oxford University Press, Oxford, 2000), p. 78.
[35] E. A. Colbourn, M. Dagenais, A. E. Douglas, and J. W. Raymonda, Can. J. Phys. **54**, 1343 (1976).
[36] R. Rydberg, Z. Phys. **73**, 376 (1931).
[37] O. Klein, Z. Phys. **76**, 226 (1932).
[38] A. L. G. Rees, Proc. Phys. Soc. London **59**, 998 (1947).
[39] J. F. Ogilvie, *The Vibrational and Rotational Spectrometry of Diatomic Molecules* (Academic Press, New York, 1998).
[40] G. Wentzel, Z. Phys. **38**, 518 (1926).
[41] H. A. Kramers, Z. Phys. **39**, 828 (1926).
[42] L. Brillouin, J. Phys. Radium **7**, 135 (1926).
[43] H.-J. Werner, P. J. Knowles, J. Almlöf, R. Lindh, F. R. Manby, M. Schütz, P. Celani, T. Korona, G. Rauhut, R. D. Amos, A. Bernhardsson, A. Berning, D. L. Cooper, M. J. O. Deegan, A. J. Dobbyn, F. Eckert, C. Hampel, G. Hetzer, A. W. Lloyd, S. J. McNicholas, W. Meyer, M. E. Mura, A. Nicklaß, P. Palmieri, R. Pitzer, U. Schumann, H. Stoll, A. J. Stone, R. Tarroni, and T. Thorsteinsson, MOLPRO, a package of *ab initio* programs.
[44] J. K. Knipp, Phys. Rev. **53**, 734 (1938).
[45] T. Y. Chang, Rev. Mod. Phys. **39**, 911 (1967).
[46] R. J. Le Roy, Mol. Spectrosc. (Chem. Soc., London) **1**, 113 (1973).
[47] J. O. Hirschfelder, C. F. Curtis, and R. B. Bird, *Molecular Theory of Gases and Liquids* (Wiley, New York, 1964) corrected printing.
[48] A. J. Stone, *The Theory of Intermolecular Forces* (Clarendon, Oxford, 1996).
[49] M. Medved, P. W. Fowler, and J. M. Hutson, Mol. Phys. **98**, 453 (2000).
[50] X. Chu and A. Dalgarno, J. Chem. Phys. **121**, 4083 (2004).
[51] W. H. E. Schwarz, P. Valtazanos, and K. Ruedenberg, Theor. Chim. Acta **68**, 471 (1985).
[52] W. H. E. Schwarz, K. Ruedenberg, and L. Mensching, J. Am. Chem. Soc. **111**, 6926 (1989).
[53] L. Mensching, W. Von Niessen, P. Valtazanos, K. Ruedenberg, and W. H. E. Schwarz, J. Am. Chem. Soc. **111**, 6933 (1989).
[54] G. C. Lie and E. Clementi, J. Chem. Phys. **60**, 1288 (1974).
[55] X. Li and J. Paldus, J. Chem. Phys. **125**, 164107 (2006).
[56] O. L. Polyansky, A. G. Császár, S. V. Shirin, N. F. Zobov, P. Barletta, J. Tennyson, D. W. Schwenke, and P. J. Knowles, Science **299**, 539 (2003).
[57] W. Cardoen and R. J. Gdanitz, J. Chem. Phys. **123**, 024304 (2005).
[58] T. A. Ruden, T. Helgaker, P. Jørgensen, and J. Olsen, J. Chem. Phys. **121**, 5874 (2004).
[59] S. Hirata, T. Yanai, R. J. Harrison, M. Kamiya, and P.-D. Fan, J. Chem. Phys. **126**, 024104 (2007).
[60] G. Tarczay, A. G. Császár, W. Klopper, and H. M. Quiney, Mol. Phys. **99**, 1769 (2001).
[61] N. C. Handy and A. M. Lee, Chem. Phys. Lett. **252**, 425 (1996).
[62] J. Gauss, A. Tajti, M. Kállay, J. F. Stanton, and P. G. Szalay, J. Chem. Phys. **125**, 144111 (2006).